

Coherent spin control of s-, p-, d- and f-electrons in a silicon quantum dot

R. C. C. Leon,^{1,*} C. H. Yang,¹ J. C. C. Hwang,^{1,†} J. Camirand Lemyre,² T. Tantt,¹ W. Huang,¹ K. W. Chan,^{1,‡} K. Y. Tan,^{3,‡} F. E. Hudson,¹ K. M. Itoh,⁴ A. Morello,¹ A. Laucht,¹ M. Pioro-Ladrière,^{2,5} A. Saraiva,^{1,§} and A. S. Dzurak^{1,¶}

¹*Center for Quantum Computation and Communication Technology,
School of Electrical Engineering and Telecommunications,
The University of New South Wales, Sydney, NSW 2052, Australia.*

²*Institut Quantique et Département de Physique,*

Université de Sherbrooke, Sherbrooke, Québec J1K 2R1, Canada

³*QCD Labs, COMP Centre of Excellence, Department of Applied Physics, Aalto University, 00076 AALTO, Finland*

⁴*School of Fundamental Science and Technology, Keio University,
3-14-1 Hiyoshi, Kohokuku, Yokohama 223-8522, Japan.*

⁵*Quantum Information Science Program, Canadian Institute for Advanced Research, Toronto, ON, M5G 1Z8, Canada*

Once the periodic properties of atoms were unveiled, chemical bonds could be understood in terms of the valence of atoms. Ideally, this rationale would extend to quantum dots¹⁻⁵, and quantum computation would be performed by merely controlling electrons in the outer shell⁶. Imperfections in the semiconductor material, even at the atomic scale, disrupt this analogy between atoms and quantum dots, so that real devices seldom display such intelligible many-electron arrangement. We demonstrate here an electrostatic quantum dot that overcomes the hardships of disorder and reveals a well defined shell structure. We observe four shells (31 electrons) with multiplicities given by spin and valley degrees of freedom^{3,4,7}. We explore various fillings consisting of a single valence electron – namely 1, 5, 13 and 25 electrons – as potential qubits. An integrated micromagnet allows us to perform electrically driven spin resonance (EDSR)^{8,9}. Higher shell states are shown to be more susceptible to the driving field, leading to faster Rabi rotations of the qubit. We investigate the impact of orbital excitations of the p and d-shell electrons¹⁰ on single qubits as a function of the dot deformation. This allows us to tune the dot excitation spectrum and exploit it for faster qubit control. Furthermore, hotspots arising from this tunable energy level structure provide a pathway towards fast spin initialisation.

Qubit architectures based on electron spins in gate defined quantum dots benefit from controllability, where single and multi-qubit coherent operations realized solely with electrical and magnetic manipulation. Furthermore, their direct compatibility with silicon microelectronics fabrication offers unique scale-up opportunities¹¹. However, fabrication reliability and interface disorder pose challenges for single electron quantum dots. Even if the single electron regime is achievable, the lone last electron often is confined in a very small region, limiting the capabilities of electrical control and interdot tunnel coupling. Many-electron quantum dots have been proposed

as a qubit decades ago¹², with the potential of resilience to charge noise^{13,14} and a more tunable tunnel coupling strength to other qubits¹⁵. In the multielectron regime, the operation of a quantum dot is sensitive to its shape. If it is axially symmetric, the orbital energy levels will be quasi-degenerate¹⁶, which is detrimental for quantum computing. On the contrary, if the quantum dot is very elongated, a shell structure will not form, and the valence electron will not merely operate as a single spin-1/2 system¹².

The scanning electron microscope (SEM) image in Fig. 1a shows a device that forms a quantum dot at the Si/SiO₂ interface under gate G1, separated by a barrier from the reservoir set by gate G2 - see Fig. 1b for a cross-sectional representation. We first study the electronic structure of said dot from its charge stability diagram, using the technique from Ref. 17, which maps out each electron transition between quantum dot and reservoir as a function of gate potential. Figure 1c shows an extremely regular set of electron transitions, revealing a quantum dot that can be occupied by up to 31 electrons with no charge trap transitions at the Si/SiO₂ interface. This range is slightly better than other devices based on similar technology¹⁸. Additional charge transitions in Fig. 1c (faint horizontal lines) arise from states between the reservoir and the quantum dot and does not affect the qubit operation. Lowering the voltage of gate G2 confines the quantum dot further and changes its eccentricity in the x-y plane.

The cut shown in Fig. 1c allows us to investigate the addition energies, i.e. the energy necessary to add the N -th electron to a dot that contains $N-1$ electrons, as seen in Fig. 1d. The first observable effect is that the charging energy is roughly inversely proportional to the number of electrons, which is a consequence of the dot size becoming larger as the dot fills up. Furthermore, very distinct peaks appear at transitions $4 \rightarrow 5$, $12 \rightarrow 13$, and $24 \rightarrow 25$. To understand the significance of these electron numbers, one may refer to the Fock-Darwin energy levels^{19,20}, where the internal spin (\uparrow, \downarrow) and valley (v_+, v_-) quantum numbers give the multiplicity of each orbital state¹. As a result, a full shell is formed when

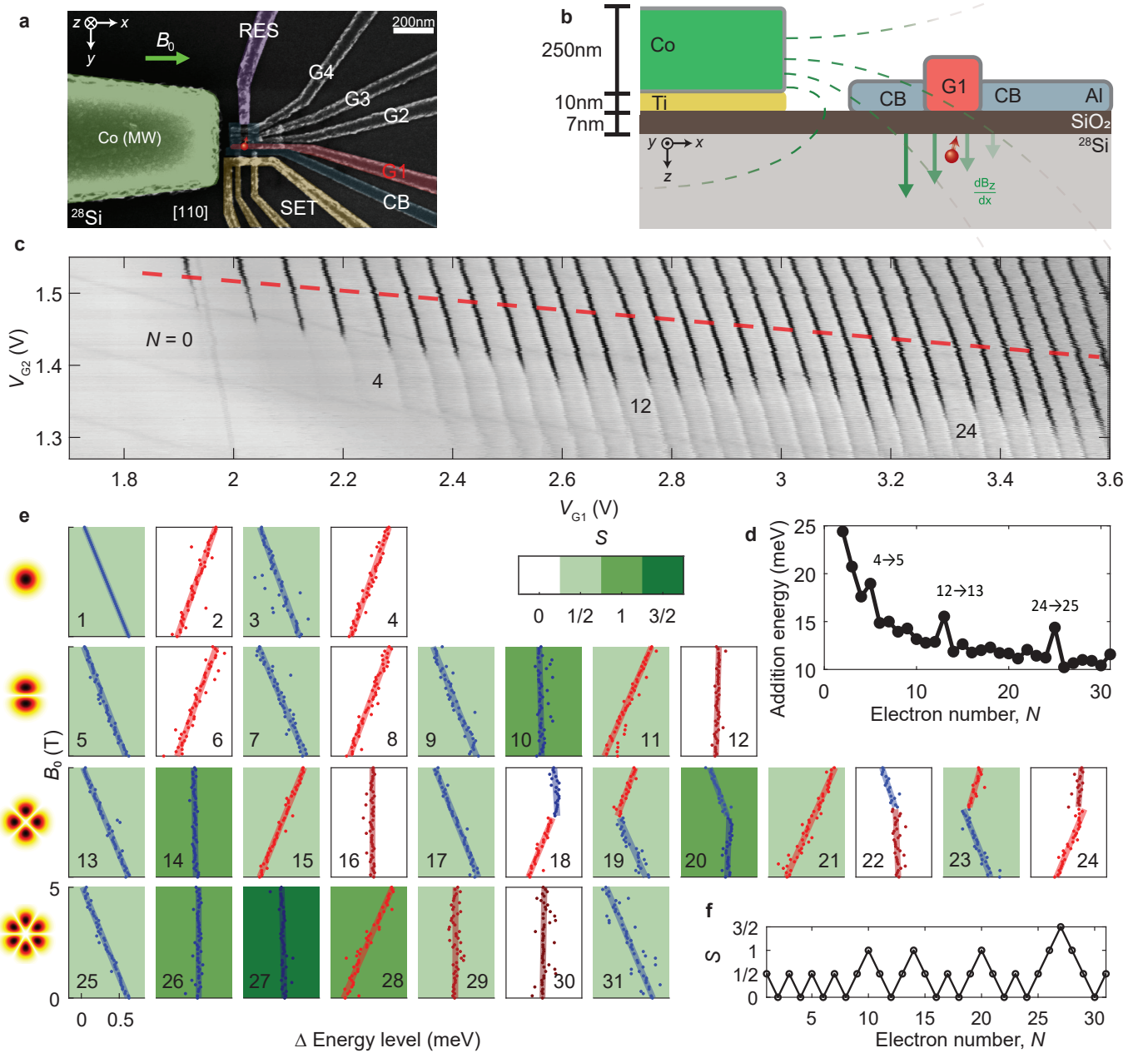


Figure 1 | Device overview and electron occupancy measurement. **a**, False-coloured SEM image of a nominally identical device. A quantum dot is formed under G1 (red), where the red dot is located. Gate RES is connected to an n-doped reservoir to load/unload electrons to/from the quantum dot, with tunnel rates controlled by G2, G3 and G4. Gate CB serves as a confinement barrier. Cobalt acts as a micromagnet and electrode for EDSR control (green). **b**, Cross sectional schematic of the device fabricated on a purified silicon-28 epi-layer (800 ppm). **c**, Pulsed lock-in signal from SET sensor I_{pulse} vs V_{G1} and V_{G2} . A square wave with peak-to-peak amplitude of 2 mV is applied to G1 for lock-in excitation, forming a charge stability diagram at $B_0 = 0$ T. Dynamic compensation is applied to the SET sensor to maintain the readout sensitivity. Electron numbers N for full shells are written on the diagram. Note that the faint gradual charge transitions in the background correspond to non-uniform 2D electron gas at the reservoir and do not affect the experiment. **d**, Charging energies along the red line in (c) in the tightly confined regime, where dot-to-reservoir or interdot transitions do not affect the system. **e**, Magnetospectroscopy of the first 31 electrons occupied in the quantum dot, up to $B_0 = 5$ T, with background colour of each plot representing spin state S at $B_0 = 0$ T. Difference in energy between adjacent electron occupancies are measured and fitted with straight lines. Note that the plot number 1 is an estimated difference in energy between the first electron and a virtual spin up electron in the previous shell. Each row of the array of plots belongs to the same shell, while each column has the same number of valence electrons on its outershell. The cartoon on the left gives an example of the electron wavefunction at each shell. **f**, Spin state of each electron occupancy extracted from (e).

there are 4, 12 and 24 electrons in the 2D quantum dot. The addition energy of the subsequent electron is larger due to the next higher orbit being filled. This is analogous to the Aufbau principle of atomic physics, that allows us to construct the electronic structure of many-electron atoms in terms of occupation of the atomic electron levels from bottom up.

In addition, a finer structure at intermediate filling is present due to the valley splitting Δ_{VS} ²¹, the energy difference between excitations along the major and minor axes of the elliptical quantum dot²² Δ_{xy} and electronic quantum correlations²³, dominated by the exchange coupling J . These energy scales are much smaller than the shell excitation, so that we can identify each set of levels by a principal quantum number. Each shell is spanned by the valley^{3,4}, spin and azimuthal¹⁰ quantum numbers. For this particular quantum dot, Δ_{VS} and Δ_{xy} may be estimated^{3,18} and both are of the order of hundreds of μeV , which is consistent with typical observations for quantum dots with similar designs⁴. Since both splittings are similar in magnitude, it is difficult to label the inner shell structure based solely on the addition energy diagram.

Magneto spectroscopy of the electron transitions (Fig. 1e) reveals the spin dependency as a function of external magnetic field strength B_0 for each electron occupancy, with cumulative spin state S presented in Fig. 1f. At lower electron occupancies, S alternates between 0 and $\frac{1}{2}$, indicating that the sequential electron loading favours anti-parallel spin states, implying $J \ll \Delta_{xy}, \Delta_{VS}$. As electron numbers increases, Hund's rule applies as some of the electrons are loaded as parallel spin, creating $S = 1$ or $\frac{3}{2}$ states, indicating $J > \Delta_{xy}, \Delta_{VS}$ in these cases. This inversion indicates that two interacting quantum dots at these fillings might lead to complex electronic states. Indeed, interdot negative exchange coupling at higher fillings has been observed in GaAs quantum dots²⁴.

We now examine the spins of monovalent dot occupations as potential qubits, i.e., the first electron of each shell $N = 1, 5, 13$ and 25 , which we call s-, p-, d- and f-electrons, respectively, in reference to the electronic orbitals. To demonstrate single qubit control, we designed this device with the capability to perform electrically-driven spin resonance (EDSR). A cobalt micromagnet positioned near the device induces a magnetic field gradient. An external uniform magnetic field $B_0 = 1.4$ T provides a Zeeman splitting between spin states for spin to charge conversion readout²⁵. This field also fully magnetises the cobalt²⁶, leading to a field gradient of approximately $1 \text{ T}/\mu\text{m}$ in the direction transverse to the quantization axis. This provides the means to drive spin flips without the need for an AC magnetic field²⁷⁻²⁹. Instead, a 40 GHz sinusoidal voltage is applied directly to the magnet. The antenna-like structure creates an AC electric field at the quantum dot, so that the electron wavefunction oscillates spatially within the slanted magnetic field, which drives Rabi oscillations of the qubit^{8,30}.

In order to initialize, control and readout the spins,

the pulse sequence depicted in Fig. 2a is performed. The amplitude and duration of the driving AC electric field is used to implement various single qubit logical gates. The fidelity of these qubit operations under the decoherence introduced by the environment is probed by a randomized benchmarking protocol^{31,32}. Supplementary Figure compares the performance of s-, p- and d-electrons. Single qubit elementary gate fidelities improve from 98.5 % to 99.7 % when the electron occupancy increases from 1 to 5 and 13 electrons. Part of the reason for this improvement is the softening of the quantum dot confinement at higher occupations – the Coulomb repulsion due to electrons in inner shells leads to a shallower confinement, thus reducing charging and orbital energies (Fig. 1d) and ultimately leading to faster Rabi frequencies (Fig. 2b inset).

Perhaps more interestingly, the improved performance of single qubits at p- and d-levels can also be attributed to a better protection against the environment in multielectron dots. Indeed, early theoretical work indicates that the inner cloud of electrons may act as a protection against decoherence, creating some shielding against electrical noise¹⁴. A better way to probe the effects of faster gating times and slower decoherence is by observing the Q -factor ($Q = T_2^{\text{Rabi}}/T_\pi$) of Rabi oscillations of 1, 5, 13 and 25 electrons in Fig. 2b, which shows close to an order of magnitude increase in Q from 1 to 5 and 13 electrons. Moreover, Rabi Chevrons in Fig. 2c-e for 1, 5 and 13 electrons indicate a visible improvement in the pattern quality of both $N = 5$ and 13 compared to $N = 1$.

Although Rabi oscillations are present for $N = 25$ in Fig. 2b, we observed its optimal π -pulse time and T_2^{Rabi} to be similar to $N = 1$. This indicates that higher shell numbers do not necessarily benefit qubit operation, as more relaxation hotspots will arise with increased multiplicity of the shell state¹⁸.

One should note that the Dresselhaus spin-orbit coupling, which is dominant in Si, has very distinct impact on each valley state, which could potentially affect the spin-orbit driven EDSR^{33,34}. Since our EDSR approach adopts an inhomogeneous magnetic field induced by a micromagnet, however, we expect that possible suppressions of spin-orbit effect by valley interference are overcome by the field gradient. In other words, the observed improvement of the Rabi oscillations is unlikely to be largely stemming from variations in the valley structure among shells.

Although multielectron quantum dots can be exploited to improve qubit performance, they raise new questions regarding the many-body physics of these dots. One particular concern is that the presence of low-lying excited orbital states may intervene with the spin dynamics. We track the excited states by altering the dot aspect ratio without changing its occupancy³⁵, adjusting the G1 and G2 gate voltages parallel to the transition lines in Fig. 1c. Firstly, we measure the resonance frequencies while varying the dot shape, as shown in Fig. 3c. Non-linear Stark-shifts are observed for $N = 1$ (Fig. 3d), 5 (Fig. 3g) and

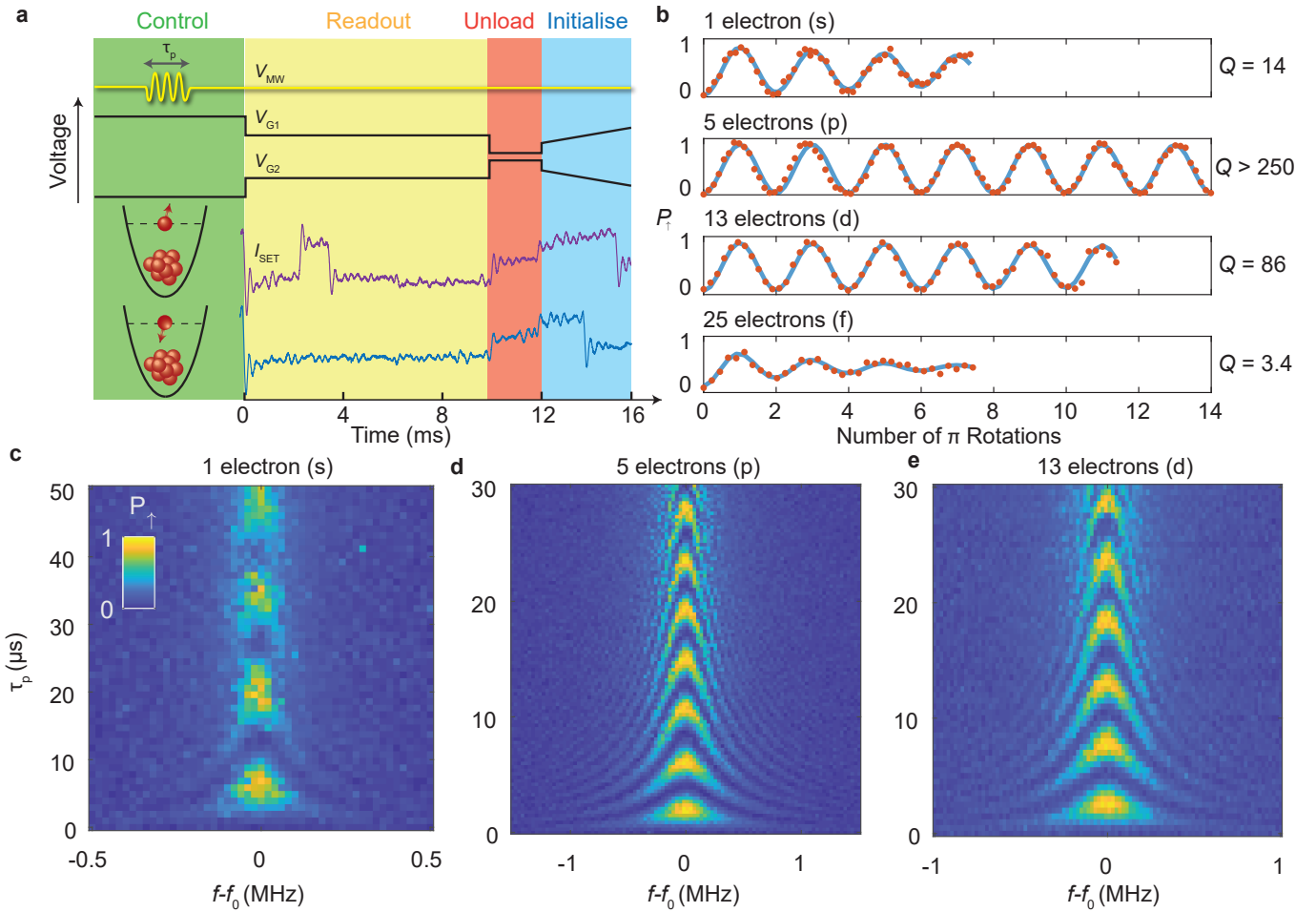


Figure 2 | Coherent spin control. **a**, Complete gate and microwave pulse sequence for single qubit control and readout. The bottom section shows the change in SET current when a valence electron is in either a spin up or down state. **b**, Rabi oscillation of 1, 5, 13 and 25 electrons. Traces for s, p, d electrons are extracted from (c-e) at $f - f_0 = 0$ MHz. Horizontal axis is number of π rotations ($\frac{T_p}{T_\pi}$) of each oscillation. $Q = \frac{T_2^{\text{Rabi}}}{T_\pi}$ for each electron occupancies is shown on the right column. **c-e**, Probability of spin up as a function of ESR frequency detuning and duration of microwave pulse for (c) $N = 1$, (d) $N = 5$ and (e) $N = 13$ electrons, performed along the grey dashed line in Fig. 3(d-l). Resonance frequencies f_0 for $N = 1, 5$ and 13 are 41.829, 41.879 and 41.827 GHz, respectively.

13 electrons (Fig. 3j), where a drop in resonance frequencies occurs at certain values of ΔV_{G1} and ΔV_{G2} (in the region near the grey lines in Fig. 3d-l, which mark the operation point at which all data is taken, unless specified otherwise). Moreover, for $N = 5$ and 13 electrons, Fig. 3i,l show that the Rabi frequencies of these two configurations are also significantly enhanced at these ΔV_G values. These are indications that the quantum dot is coupled to states of different nature at these dot conformations. There are no charge transitions (or visible features in the charge stability diagram), confirming that the ground state configuration is left unchanged. Note that such Rabi frequency enhancement is also observed in $N = 1$ electron configuration, but it is still an order of magnitude lower than 5 and 13 electrons.

The quantum mechanical description of EDSR involves virtual excitations (valley³⁶ or orbital³⁷). This indicates

that the changes observed in Fig. 3 are related to the influence of an upper level approaching the ground state. We confirm this interpretation by measuring the spin relaxation time T_1 through the pulse sequence in Fig. 3b, as shown in Fig. 3e,h,k. The presence of an excited orbital or valley state nearby the Zeeman excitation generates a hotspot for relaxation, which is in the order of 10 ms, similar to previous literature^{18,38,39}. We may exploit this control over the spectrum to induce fast relaxation on demand for qubit initialization, operate the qubit where f_{Rabi} is high, and store it in the long T_1 configuration. The power of the EDSR drive did not show significant impact on the observed values of Q factor, contrary to recent observations in depletion mode quantum dot experiments⁴⁰.

Figure 3h also shows an additional relaxation hotspot around $\Delta V_{G1} = 0$ mV for the d-shell qubit. This is most

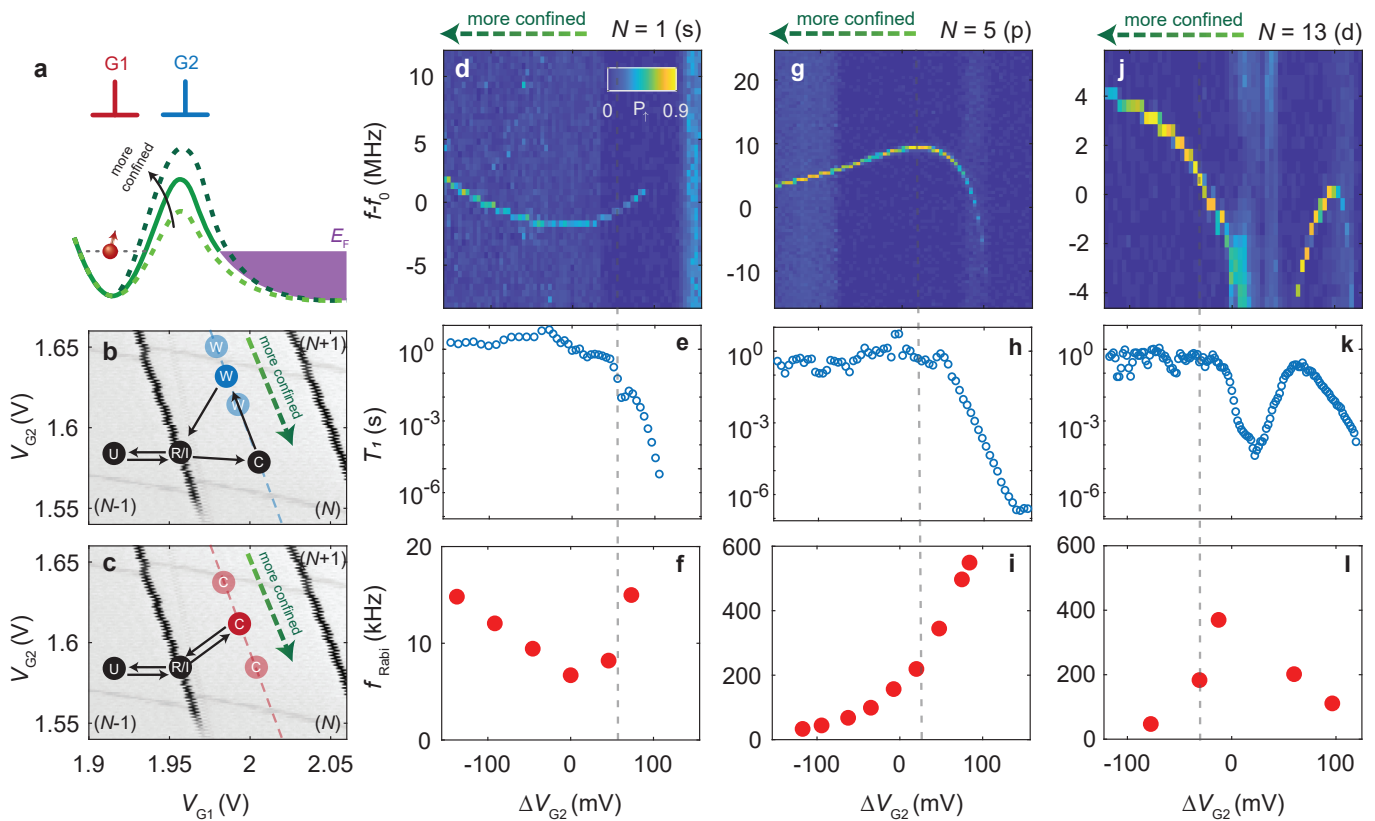


Figure 3 | Starkshift, tunable Rabi frequency and relaxation time. **a**, Cartoon representation of the quantum device energy band diagram. G2 voltage varies in order to change the quantum dot size and tunnel rate to the reservoir (purple). Compensating voltage is also applied to G1 to maintain the quantum dot energy level relative to Fermi level E_F . **b,c**, Schematics of the pulse sequences for **(b)** T_1 relaxation, and **(c)** Rabi control experiment. The qubit control point varies along the dashed line inside the charge stability diagram, parallel to charge transition, with electron occupancy either $N = 1, 5$ or 13 . **d**, Non-linear Starkshift of qubit resonance frequency is observed when the qubit control point changes along dashed line in **(b)** and **(c)**, for $N = 1$ electron. At certain voltage levels, the resonance frequency shifts dramatically and eventually qubit readout is unachievable. **e**, Correlation is observed between the magnitude of the differential ESR resonance frequency and qubit relaxation time T_1 . **f**, Correlation is observed between change in magnitude of ESR resonance frequency and Rabi frequency f_{Rabi} . Maximum Rabi frequency is obtained when the change in ESR frequency $|\frac{\Delta f}{\Delta V_{G2}}|$ is maximised. **g-l**, Starkshift, T_1 and Rabi frequencies similar to **(d-f)**, but for **(g-i)** $N = 5$ and **(j-l)** 13 electrons. $f_0 = 41.835, 41.870, 41.826$ GHz for $N = 1, 5$ and 13 electrons, respectively.

likely due to the added orbital near degeneracy at the d-shells, which implies more pathways for qubit relaxation. This near-degeneracy could also explain why the 10 and 14 electron configuration have a triplet ground state²⁴ (see the total spin state in Fig. 1g). We mention that these higher total spin states are observed to also be coherently drivable, but this exceeds the scope of present work (see Extended Fig. 1c & d).

The present work experimentally demonstrates that purely spin-based qubits may be implemented in multi-electron quantum dots. This could be a desirable feature as long as the shell structure is well preserved, such as in very small SiMOS electrostatic quantum dots. Operation based on EDSR takes advantage of the extended wavefunction to drive the qubit with higher control fidelity and longer distance J coupling between qubits. A multi-electron system results in a richer many-body exci-

tation spectrum, which could have higher Rabi frequencies for fast qubit gates and enhanced relaxation rates for quick qubit initialization. We anticipate the possibility of complex two qubit physics, with a possible singlet-triplet inversion²⁴, mimicking the physics of paramagnetic bonding⁴¹. This would require a revision of the two qubits gate strategies, as well as the spin-to-charge conversion techniques for qubit read-out.

ACKNOWLEDGMENTS

We acknowledge support from the Australian Research Council (CE170100012), and the NSW Node of the Australian National Fabrication Facility. The views and conclusions contained in this document are those of the authors and should not be interpreted as representing

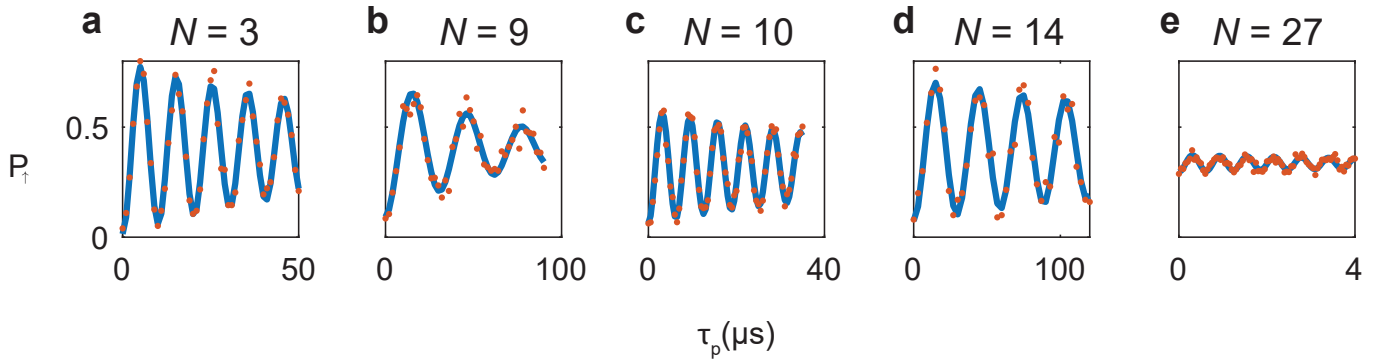
the official policies, either expressed or implied, of the Army Research Office or the U.S. Government. The U.S. Government is authorized to reproduce and distribute reprints for Government purposes notwithstanding any copyright notation herein. J. C. and M. P. acknowledge support from the Canada First Research Excellence Fund

and in part by the National Science Engineering Research Council of Canada. K. Y. T. acknowledges support from the Academy of Finland through project Nos. 308161, 314302 and 316551.

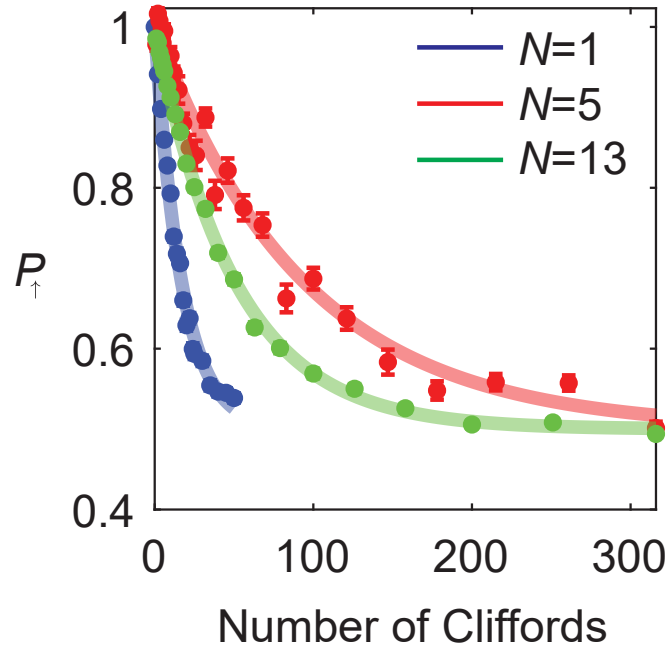
The authors declare that they have no competing financial interests.

- * ross.leon@unsw.edu.au
- † Current address: Research and Prototype Foundry, The University of Sydney, Sydney, NSW 2006, Australia.
- ‡ Current address: Microsoft Quantum, The University of Sydney, Sydney, NSW 2006, Australia.
- § a.saraiva@unsw.edu.au
- ¶ a.dzurak@unsw.edu.au
- 1 Tarucha, S., Austing, D. G., Honda, T., Van Der Hage, R. J. & Kouwenhoven, L. P. Shell Filling and Spin Effects in a Few Electron Quantum Dot. *Physical Review Letters* **77**, 3613–3616 (1996). URL <https://journals.aps.org/prl/pdf/10.1103/PhysRevLett.77.3613>.
 - 2 Rontani, M. *et al.* Full configuration interaction approach to the few-electron problem in artificial atoms. *The Journal of chemical physics* **124**, 124102 (2006). URL <http://aip.scitation.org/toc/jcp/124/12>.
 - 3 Borselli, M. G. *et al.* Measurement of valley splitting in high-symmetry Si/SiGe quantum dots. *Applied Physics Letters* **98**, 123118 (2011).
 - 4 Yang, C. H. *et al.* Orbital and valley state spectra of a few-electron silicon quantum dot. *Physical Review B* **86**, 115319 (2012). URL <https://journals.aps.org/prb/pdf/10.1103/PhysRevB.86.115319https://link.aps.org/doi/10.1103/PhysRevB.86.115319>.
 - 5 Liles, S. D. *et al.* Spin and orbital structure of the first six holes in a silicon metal-oxide-semiconductor quantum dot. *Nature Communications* **9**, 3255 (2018). URL <http://www.nature.com/articles/s41467-018-05700-9>.
 - 6 Higginbotham, A. P., Kuemmeth, F., Hanson, M. P., Gosard, A. C. & Marcus, C. M. Coherent operations and screening in multielectron spin qubits. *Physical review letters* **112**, 26801 (2014).
 - 7 Lim, W. H. *et al.* Spin filling of valley-orbit states in a silicon quantum dot. *Nanotechnology* **22**, 335704 (2011). URL <http://iopscience.iop.org/article/10.1088/0957-4484/22/33/335704/pdf>.
 - 8 Pioro-Ladrière, M. *et al.* Electrically driven single-electron spin resonance in a slanting Zeeman field. *Nature Physics* **4**, 776–779 (2008). URL <http://www.nature.com/doi/10.1038/nphys1053http://dx.doi.org/10.1038/nphys1053http://www.nature.com/articles/nphys1053>. 0805.1083.
 - 9 Kawakami, E. *et al.* Electrical control of a long-lived spin qubit in a Si/SiGe quantum dot. *Nature Nanotechnology* **9**, 666–670 (2014). URL <http://www.nature.com/articles/nnano.2014.153>.
 - 10 Jacak, L., Hawrylak, P., Wojs, A., Wójs, A. & Wojs, A. *Quantum dots* (Springer Science & Business Media, 2013). URL <https://link.springer.com/content/pdf/bfm%7B3A978-3-642-72002-4%7D2F1.pdf>.
 - 11 Vandersypen, L. M. K. *et al.* Interfacing spin qubits in quantum dots and donorshot, dense, and coherent. *npj Quantum Information* **3**, 34 (2017). URL <http://www.nature.com/articles/s41534-017-0038-y>.
 - 12 Hu, X. & Das Sarma, S. Spin-based quantum computation in multielectron quantum dots. *Physical Review A - Atomic, Molecular, and Optical Physics* **64**, 042312 (2001). URL <https://link.aps.org/doi/10.1103/PhysRevA.64.042312>. 0101102.
 - 13 Barnes, E., Kestner, J. P., Nguyen, N. T. T. & Sarma, S. D. Screening of charged impurities with multielectron singlet-triplet spin qubits in quantum dots. *Physical Review B* **84**, 235309 (2011).
 - 14 Bakker, M. A., Mehl, S., Hiltunen, T., Harju, A. & DiVincenzo, D. P. Validity of the single-particle description and charge noise resilience for multielectron quantum dots. *Physical Review B* **91**, 155425 (2015).
 - 15 Harvey-Collard, P. *et al.* Coherent coupling between a quantum dot and a donor in silicon. *Nature Communications* **8**, 1029 (2017). URL <http://www.nature.com/articles/s41467-017-01113-2>.
 - 16 Kouwenhoven, L. P. *et al.* Excitation spectra of circular, few-electron quantum dots. *Science* **278**, 1788–1792 (1997).
 - 17 Yang, C. H., Lim, W. H., Zwanenburg, F. A. & Dzurak, A. S. Dynamically controlled charge sensing of a few-electron silicon quantum dot. *AIP Advances* **1**, 42111 (2011). URL <http://aip.scitation.org/doi/10.1063/1.3654496>.
 - 18 Yang, C. H. *et al.* Spin-valley lifetimes in a silicon quantum dot with tunable valley splitting. *Nature Communications* **4**, 2069 (2013). URL <http://www.nature.com/articles/ncomms3069>.
 - 19 Fock, V. Bemerkung zur Quantelung des harmonischen Oszillators im Magnetfeld. *Zeitschrift für Physik A Hadrons and Nuclei* **47**, 446–448 (1928).
 - 20 Darwin, C. G. The diamagnetism of the free electron. In *Mathematical Proceedings of the Cambridge Philosophical Society*, vol. 27, 86–90 (Cambridge University Press, 1931).
 - 21 Zwanenburg, F. A. *et al.* Silicon quantum electronics. *Reviews of Modern Physics* **85**, 961–1019 (2013). URL <https://link.aps.org/doi/10.1103/RevModPhys.85.961>.
 - 22 Ngo, C. Y., Yoon, S. F., Fan, W. J. & Chua, S. J. Effects of size and shape on electronic states of quantum dots. *Physical Review B* **74**, 245331 (2006). URL <https://link.aps.org/doi/10.1103/PhysRevB.74.245331>.
 - 23 Harting, J., Mülken, O. & Borrmann, P. Interplay between shell effects and electron correlations in quantum dots. *Physical Review B* **62**, 10207 (2000).
 - 24 Martins, F. *et al.* Negative spin exchange in a multielectron quantum dot. *Physical review letters* **119**, 227701 (2017).
 - 25 Elzerman, J. M. *et al.* Single-shot read-out of an individual electron spin in a quantum dot. *Nature* **430**, 431–435 (2004). URL <http://www.nature.com/doi/10.1038/nature02693>.

- ²⁶ Lachance-Quirion, D., Camirand Lemyre, J., Bergeron, L., Sarra-Bournet, C. & Pioro-Ladrière, M. Magnetometry of micro-magnets with electrostatically defined Hall bars. *Applied Physics Letters* **107**, 223103 (2015). URL <http://aip.scitation.org/doi/10.1063/1.4936626>. arXiv:1512.01866v1.
- ²⁷ Koppens, F. H. L. *et al.* Driven coherent oscillations of a single electron spin in a quantum dot (2006). URL http://koppensgroup.icfo.es/untitled/2006koppensdriven{}_coherent.pdf.
- ²⁸ Veldhorst, M. *et al.* An addressable quantum dot qubit with fault-tolerant control-fidelity. *Nature Nanotechnology* **9**, 981–985 (2014). URL <http://www.nature.com/articles/nnano.2014.216><http://dx.doi.org/10.1038/nnano.2014.216><http://www.nature.com/doi/10.1038/nnano.2014.216>. arXiv:1407.1950v1.
- ²⁹ Pla, J. J. *et al.* A single-atom electron spin qubit in silicon. *Nature* **489**, 541–5 (2012). URL <http://www.ncbi.nlm.nih.gov/pubmed/22992519><http://www.nature.com/articles/nature11449>. 1305.4481.
- ³⁰ Tokura, Y., Van Der Wiel, W. G., Obata, T. & Tarucha, S. Coherent single electron spin control in a slanting zeeman field. *Physical Review Letters* **96** (2006). URL <https://journals.aps.org/prl/pdf/10.1103/PhysRevLett.96.047202>. 0510411.
- ³¹ Knill, E. *et al.* Randomized benchmarking of quantum gates. *Physical Review A* **77**, 12307 (2008). URL <https://link.aps.org/doi/10.1103/PhysRevA.77.012307>.
- ³² Magesan, E., Gambetta, J. M. & Emerson, J. Scalable and Robust Randomized Benchmarking of Quantum Processes. *Physical Review Letters* **106**, 180504 (2011). URL <https://link.aps.org/doi/10.1103/PhysRevLett.106.180504>.
- ³³ Nowack, K. C., Koppens, F. H. L., Nazarov, Y. V. & Vandersypen, L. M. K. Coherent control of a single electron spin with electric fields. *Science (New York, N.Y.)* **318**, 1430–3 (2007). URL <http://www.ncbi.nlm.nih.gov/pubmed/17975030>.
- ³⁴ Corna, A. *et al.* Electrically driven electron spin resonance mediated by spinvalleyorbit coupling in a silicon quantum dot. *npj Quantum Information* **4**, 6 (2018). URL <http://www.nature.com/articles/s41534-018-0059-1>.
- ³⁵ Hwang, J. C. C. *et al.* Impact of g -factors and valleys on spin qubits in a silicon double quantum dot. *Physical Review B* **96**, 045302 (2017). URL <http://link.aps.org/doi/10.1103/PhysRevB.96.045302>.
- ³⁶ Hao, X., Ruskov, R., Xiao, M., Tahan, C. & Jiang, H. Electron spin resonance and spin–valley physics in a silicon double quantum dot. *Nature communications* **5**, 3860 (2014).
- ³⁷ Rashba, E. I. Theory of electric dipole spin resonance in quantum dots: Mean field theory with Gaussian fluctuations and beyond. *Physical Review B* **78**, 195302 (2008).
- ³⁸ Srinivasa, V., Nowack, K. C., Shafei, M., Vandersypen, L. M. K. & Taylor, J. M. Simultaneous Spin-Charge Relaxation in Double Quantum Dots. *Physical Review Letters* **110**, 196803 (2013). URL <https://link.aps.org/doi/10.1103/PhysRevLett.110.196803>.
- ³⁹ Borjans, F., Zajac, D. M., Hazard, T. M. & Petta, J. R. Single-Spin Relaxation in a Synthetic Spin-Orbit Field (2018). URL <http://arxiv.org/abs/1811.00848><https://arxiv.org/pdf/1811.00848.pdf>.
- ⁴⁰ Takeda, K. *et al.* A fault-tolerant addressable spin qubit in a natural silicon quantum dot. *Science Advances* **2**, e1600694 (2016). URL <http://advances.sciencemag.org/lookup/doi/10.1126/sciadv.1600694>.
- ⁴¹ Lange, K. K., Tellgren, E. I., Hoffmann, M. R. & Helgaker, T. A paramagnetic bonding mechanism for diatomics in strong magnetic fields. *Science (New York, N.Y.)* **337**, 327–331 (2012). URL <http://www.ncbi.nlm.nih.gov/pubmed/22822146>.



Extended Figure 1 | Coherent control at various electron occupancies. Rabi oscillations at different electron numbers N inside the a single quantum dot. (a) $N = 3$ (b) $N = 9$ (c) $N = 10$ (d) $N = 14$ (e) $N = 27$. Note that from Fig. 1f, $N = 10$ and 14 electrons have total spin states $S = 1$, while $N = 27$ electrons has $S = \frac{3}{2}$.



Extended Figure 2 | Randomised benchmarking. Single qubit randomised benchmarking at for $N = 1, 5$ and 13 electrons, with elementary gate fidelities of 98.5 %, 99.7 % and 99.5 %, respectively